NIH Public Access
Author Manuscript
J Am Chem Soc. Author manuscript; available in PMC 2011 December 22.

Published in final edited form as:
J Am Chem Soc. 2010 December 22; 132(50): 17733–17740. doi:10.1021/ja103998v.

Role of the Azadithiolate Cofactor in Models for the [FeFe]-Hydrogenase: Novel Structures and Catalytic Implications

Matthew T. Olsen, **Thomas B. Rauchfuss***, and **Scott R. Wilson**
Department of Chemistry, University of Illinois at Urbana-Champaign, Urbana, IL 61801

Abstract

The report summarizes studies on the redox behavior of synthetic models for the [FeFe]-hydrogenases, consisting of diiron dithiolato carbonyl complexes bearing the amine cofactor and its *N*-benzyl derivative. Of specific interest are the causes of the low reactivity of oxidized models toward H_2, which contrasts with the high activity of these enzymes for H_2 oxidation. The redox and acid-base properties of the model complexes $[Fe_2[(SCH_2)_2NR](CO)_3(dppv)(PMe_3)]^+$ ($[\mathbf{2}]^+$ for R = H and $[\mathbf{2'}]^+$ for R = $CH_2C_6H_5$, dppv = *cis*-1,2-bis(diphenylphosphino)ethylene)) indicate that addition of H_2 and followed by deprotonation are (i) endothermic for the mixed valence ($Fe^{II}Fe^{I}$) state and (ii) exothermic for the diferrous ($Fe^{II}Fe^{II}$) state. The diferrous state is shown to be unstable with respect to coordination of the amine to Fe, a derivative of which was characterized crystallographically. The redox and acid-base properties for the mixed valence models differ strongly for those containing the amine cofactor versus those derived from propanedithiolate. Protonation of $[\mathbf{2'}]^+$ induces disproportionation to a 1:1 mixture of the ammonium-$Fe^{I}Fe^{I}$ and the dication $[\mathbf{2'}]^{2+}$ ($Fe^{II}Fe^{II}$). This effect is consistent with substantial enhancement of the basicity of the amine in the $Fe^{I}Fe^{I}$ state vs the $Fe^{II}Fe^{I}$ state. The $Fe^{I}Fe^{I}$ ammonium compounds are rapid and efficient H-atom donors toward the nitroxyl compound TEMPO. The atom transfer is proposed to proceed via the hydride, as indicated by the reaction of $[HFe_2[(SCH_2)_2NH](CO)_2(dppv)_2]^+$ with TEMPO. Collectively, the results suggest that proton-coupled electron-transfer pathways should be considered for H_2 activation by the [FeFe]-hydrogenases.

Introduction

The catalytic chemistry of hydrogen evolution and oxidation is topical because H_2 is a versatile reagent and a promising carrier of energy.[1, 2] New approaches to this area of catalysis have been inspired by the hydrogenase enzymes, and studies on the [FeFe]-hydrogenases have proven especially influential.[3] We and others have proposed that catalysis occurs at a single coordination site on one Fe center of the diiron subunit (Figure 1),[4,5] with participation of various cofactors.

Ongoing research in this area focuses on elucidating the electronic features of the bimetallic site – oxidation state, redox potentials, asymmetry - *and* equipping models with the cofactors required for efficient catalysis. Thus, models have evolved from the simple $Fe_2(SR)_2(CO)_6$ to substituted derivatives $Fe_2(SR)_2(CO)_{6-x}L_x$ which exhibit the two essential attributes of hydrogenases – the acid-base and redox behavior. Two cofactors are of functional significance since they enhance the redox or acid-base properties inherent in the diiron center. First, the redox-active 4Fe-4S cluster allows the diiron subsite, which operates

rauchfuz@illinois.edu.

Supporting Information Available: Crystallographic information file (cif) for $[\mathbf{2'}(MeCN)](BF_4)_2$, thermodynamic calculations, and associated spectra.

NIH-PA Author Manuscript

NIH-PA Author Manuscript

NIH-PA Author Manuscript

via a $1e^-$ couple, to effect $2e^-$ redox reactions, as required by the $H_2/2H^+$ redox couple. Second, and very relevant to this report, the amine-containing dithiolate cofactor[4, 5] is proposed to relay protons to and from the distal Fe.[6]

Synthetic models differ from the diiron site in the protein in three important ways. First, most models feature organophosphorus ligands such as *cis*-1,2-$C_2H_2(PPh_2)_2$ (dppv) and PMe_3 in place of the cyanide cofactors. This change enables mechanistic studies without the complications of reactions at Fe*C*N. Second, with a single exception,[10] models omit the 4Fe-4S cofactor that is found in the 6-Fe "H-cluster" (Figure 1). Finally, the model complexes differ from the active site in the stereochemistry of one of the iron centers. In the protein, the distal Fe center adopts an "inverted" (also described as "rotated"[11]) structure in which a CO ligand occupies a semi-bridging position between the two Fe centers. This stereochemistry exposes a coordination site adjacent to the amine of the dithiolate cofactor. The inverted structure is observed in the *oxidized* models of the type $[Fe_2(SR)_2(CO)_4L_2]^+$ and $[Fe_2(SR)_2(CO)_3L_3]^+$,[12–15] but such inverted structures are rarely observed in *reduced* diiron models.[16, 17] Theoretical studies indicate that rotated structures are destabilized by about 10 kcal in model complexes.[11]

More recent models incorporate the amine cofactor, which we call azadithiolate (adt = $(SCH_2)_2NH^{2-}$). *N*-Protonation of such compounds shifts the reduction potential of the diiron center by ~0.5 V, and the oxidation potential by ~0.2 V.[18, 19] Of relevance to the enymatic mechanism, the complex $Fe_2(adt)(CO)_2(dppv)_2$ electrocatalyzes hydrogen evolution from weaker acids than is possible for the related complexes lacking the amine, e.g. $Fe_2(pdt)(CO)_2(dppv)_2$ (pdt = $S_2(CH_2)_3^{2-}$).[6] Catalysis by these electron-rich models proceeds via the intermediacy of an iron hydride, for which the rates of formation and deprotonation are modified by the amine. Such amine-complemented models for the H_{ox} state are ideal systems to explore factors relevant to H_2 oxidation. In the present report, we examine the interplay between the acid-base behavior of the amine and the redox properties of the Fe_2 centers in $Fe_2(adt)(CO)_3(dppv)(PMe_3)$.[9] Protonation of $Fe_2(adt)(CO)_3(dppv)(PMe_3)$ gives the ammonium derivative as the only spectroscopically detectable tautomer. Via a first order pathway, the ammonium compound tautomerizes slowly at room temperature in CH_2Cl_2 solution to the isomeric "μ-hydride," which feature H^- bound to both Fe centers (Scheme 1).[9, 20]

In contrast to the "trisphosphine", the tetrasubstituted diiron dithiolates form spectroscopically detectable terminal hydrides. The enzyme is thought to operate via such terminal hydrides, not μ-hydrides. For $[HFe_2(adt)(CO)_2(dppv)_2]BF_4$, the pK_a ^{CD_2Cl_2} is between 5.7 and 8.2.[6] The terminal hydride and ammonium tautomers of this complex coexist in comparable amounts in CH_2Cl_2 solution (Scheme 1). Indicative of the subtleties of this system is the finding that high concentrations of BF^{4-} shift the equilibrium from the hydride toward the ammonium tautomer.[6]

The process by which H_2 is activated by diiron dithiolato complexes came into focus with the finding that H_2 is only slowly oxidized by $[Fe_2(adt)(CO)_3(dppv)(PMe_3)]^+$ (at 2000 psi H_2, rate ~ 10^{-4} s^{-1})[9], whereas the enzyme from *D. gigas* oxidizes H_2 at 10^5 s^{-1}.[21] The low reactivity of mixed valence models toward H_2 is generally understandable because the heterolytic scission of H_2 by iron characteristically requires ferrous centers.[1] Theoretical studies show that the diferrous state of the diiron subsite is well suited for activation of H_2.[22] Diferrous μ-hydride complexes catalyzes H-D exchange between H_2 and D_2O, albeit only photochemically.[23] Diferrous compounds that contain a vacant coordination site are rare,[24, 25] and mononuclear ferrous ν^2-H_2 complexes have much precedence.[26, 27] Furthermore, amine-complemented mononuclear ferrous phosphine complexes have been shown to under redox-triggered tautomerization (eq 1).[28]

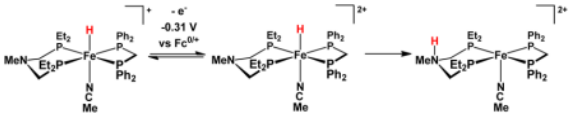

(1)

Results

Synthesis and Characterization of Diferrous κ^3-Azadithiolato Complexes

On a preparative scale and consistent with ample precedent,[12–15] oxidation of $Fe_2[(SCH_2)_2X](CO)_3(dppv)(PMe_3)$ with Fc^+ was found to yield the mixed valence $Fe^{II}Fe^{I}$ derivatives ("H_{ox} models"), where X = CH_2, NH, NBn, O, for **1**, **2**, **2′**, **3**, respectively (Bn = $CH_2C_6H_5$).[9, 12] These cationic derivatives are stabilized by bulky arylborate counteranions, which are essential for the stabilization of the oxidized azadithiolates.[9] The azadithiolates were found to undergo a second oxidation with $FcBAr^F_4$, and in this way we generated [**2′**]$(BAr^F_{24})_2$ ($FcBAr^F_4$ = $[Fe(C_5H_5)_2]B(C_6H_3\text{-}3,5\text{-}(CF_3)_2)_4$). The ^{31}P NMR spectrum indicates that[**2′**]$(BAr^F_4)_2$ is diamagnetic and C_s-symmetric. The nu;$_{CO}$ bands are shifted to higher energy by ~40 cm^{-1} from the position for [**2′**]$^+$, and all three bands occur in the terminal carbonyl region (2066, 2008, and 1977 cm^{-1}). When we instead employed the oxidant $FcBF_4$, a spectroscopically distinct compound was observed (Supporting Information).

Treatment of a CD_2Cl_2 solution of [**2′**]$^{2+}$ with MeCN was found to afford stable adducts, regardless of the counteranion, of the formula [**2′**(NCMe)]$^{2+}$. Although the $BAr^F_4{}^-$ salts afforded tacky oils, the $BF_4{}^-$ salts readily crystallized. The crystallographic analysis of this salt revealed a diiron dithiolate as expected, but that unlike all previously reported azadithiolato complexes,[29–31] the amine is coordinated to Fe (Figure 2). The Fe---Fe distance of 3.447(2) Å is nonbonding, which is also uncommon.[24, 32–34] The two iron centers, which are still linked by a pair of thiolates, are each octahedral. The coordination spheres of the Fe subsites are described as $Fe(CO)_2(PMe_3)(NCMe)(SR)_2$ and Fe(CO)(dppv)(amine)$(SR)_2$. The S-Fe-N angles are acute at ~73º, but the other Fe-ligand bond lengths and angles are within the normal range (Table I).

The solution properties of [**2′**(NCMe)]$^{2+}$ were examined by variable temperature ^{31}P NMR spectroscopy. Dissolution of the crystalline [**2′**(NCMe)]$(BF_4)_2$ at −70 °C gave a compound with the same spectroscopic signature as was obtained by addition of MeCN to a CD_2Cl_2 solution of [**2′**]$(BAr^F_4)_2$ generated at −70 °C. Over the course of ~24 h at 20 °C, this species isomerized to a second symmetrical isomer (two ^{31}P NMR signals) (eq 2, Figure 3). Solutions of [**2′**]$(BAr^F_4)_2$ were found to rapidly and irreversibly form an adduct upon treatment with 1 atm of CO. In contrast, *mono*cation [**2′**]$^+$ binds CO reversibly, and the adducts are only observable at low temperatures.[9, 13] Solutions of [**2′**]$(BAr^F_4)_2$ were found to be unreactive towards H_2 at −78 °C, although more forcing conditions were precluded by the thermal sensitivity of this salt. These dications, e.g. [**2′**]$^{2+}$, react at low temperatures with $PhSiH_3$ to give hydrides such as [(μ-H)**2′**]$^+$.

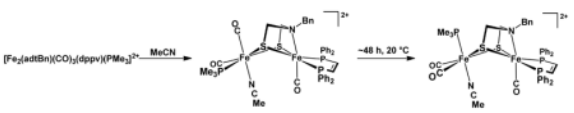

(2)

NIH-PA Author Manuscript NIH-PA Author Manuscript NIH-PA Author Manuscript

NIH-PA Author Manuscript

NIH-PA Author Manuscript

NIH-PA Author Manuscript

Electrochemical Properties of Diiron Azadithiolates

Diiron dithiolates of the formula $Fe_2[(SCH_2)_2X](CO)_3(dppv)(PMe_3)$ undergo a reversible $1e^-$ oxidation for X = CH_2, NH, $NCH_2C_6H_5$, and O (for **1**, **2**, **2′**, **3**; see Figures 4, eq 3, and Table 2). For **2′** the ratios of the oxidation and reduction currents (i_{pc}/i_{pa}) are >0.9 at a scan rate of 0.100 V/s in noncoordinating solvents (CH_2Cl_2). The linear dependence of i_p on (scan rate)$^{0.5}$ also indicates a diffusion-controlled process.

Oxidations corresponding to the $[Fe_2(SR)_2]^{+/2+}$ ($Fe^{II}Fe^{I}/Fe^{II}Fe^{II}$) couple proved highly dependent on the dithiolate (Figure 4 and eq 3). For the propane- and oxadithiolato compounds, but not the azadithiolates, a poorly reversible second oxidation is observed at 0.890±0.040 V more anodic than the $[Fe_2(SR)_2]^{o/+}$ couple. Unlike the amine-free derivatives, the $[Fe_2(SR)_2]^{+/2+}$ couple for the azadithiolates **2** and **2′** occurs at mild potentials and displayed full reversibility. Interestingly Δ*E* for **2** is significantly smaller than that for **2′**. When non-coordinating $[(C_4H_9)_4N]BAr^F{}_4$ electrolyte was employed, Δ*E* increased by 130 and 177 mV for **2′** and **2** respectively. This separation of electrochemical events is commonly observed in non-coordinating electrolytes,[35] and the larger value of Δ*E* for **2** versus **2′** is attributable to the ability of smaller fluoroanions such as PF_6^- to engage in hydrogen-bonding.[36] Upon addition of MeCN to CH_2Cl_2 solutions of **2′**, E_2 becomes irreversible and two closely spaced cathodic waves are observed at −0.80 and −0.90 V. The strong effect of MeCN is consistent with the formation of the adduct $[\mathbf{2}'(MeCN)]^{2+}$.

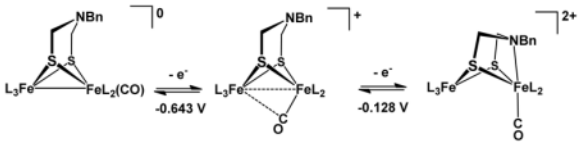

(3)

Acid-Base Reactions

The pK_a ^{CD_2Cl_2} values of the ammonium compounds $[H\mathbf{2}']^+$ and $[H\mathbf{2}]^+$ were measured as 3.3 and 3.2, respectively, by titration of **2′** and **2** with $[HPMe_2Ph]BF_4$ (pK_a ^{CD_2Cl_2} = 5.7).[37] We could not directly determine the corresponding pK_a of $[H\mathbf{2}']^{2+}$ because $[\mathbf{2}']^+$ undergoes quasi-disproportionation upon treatment with acids, even in solution at −78 °C. The product mixture consists of equal amounts of the reduced ammonium species $[H\mathbf{2}']^+$ and the dication $[\mathbf{2}']^{2+}$ (eq 4, Figure 5).

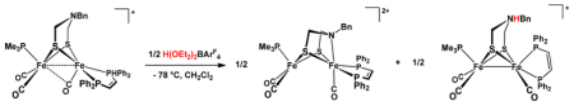

(4)

The proton-induced quasi-disproportionation of $[\mathbf{2}']^+$ (eq 4) is driven by the strong oxidizing ability of $[H\mathbf{2}']^{2+}$. The requirement of 0.5 equiv of acid for the reaction in eq 2 was confirmed. Furthermore, >0.5 equiv $H(OEt_2)_2BAr^F{}_4$ was found not to affect the product distribution, a result consistent with the low basicity of $[\mathbf{2}']^{2+}$, wherein the amine is coordinated to Fe. In contrast to this behavior, mixed-valence Fe(I)Fe(II) complexes *lacking* azadithiolates are unreactive towards acid. For example, a CH_2Cl_2 solution of $[Fe_2(S_2C_3H_6)(CO)_3(dppv)(PMe_3)]BAr^F{}_4$ was unaffected by treatment with $H(OEt_2)_2BAr^F{}_4$ at 20 °C.

NIH-PA Author Manuscript

NIH-PA Author Manuscript

NIH-PA Author Manuscript

Together with the pK_a for [H**2**]$^+$, $E_{1/2}$ for the [H**2**]$^{+/2+}$ couple would allow us to calculate the acidity of the mixed valence ammonium compound, i.e. pK_a for [H**2**]$^{2+}$. The [H**2**]$^{+/2+}$ couple is irreversible, thus precluding accurate determination of $E_{1/2}$. Nonetheless, estimating $E_{1/2}$ as the potential of the anodic wave at half-height would indicate that 1e$^-$ oxidation of [H**2**]$^+$ decreases the basicity of the amine by as much as 10^9 (CH_2Cl_2 solution, Scheme 2).

H-Atom Transfer Reactions

The electron-rich *N*-protonated azadithiolato complexes were found to serve as H-atom donors. Thus, treatment of [H**2′**]$^+$ with one equiv of 2,2,6,6-tetramethylpiperidin-1-oxyl (TEMPO), an H-atom abstracting agent,[38] immediately and quantitatively yielded [**2′**]$^+$ at 293 °C (eq 5, $R_2NO^{\cdot}$ = TEMPO). This reaction is conveniently monitored by IR spectroscopy in the nu;$_{CO}$ region.

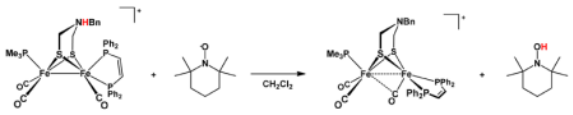

(5)

When the reaction was monitored by *in-situ* IR spectroscopy at low temperatures, a transient build-up of **2′** was detected. This species results from the reversible deprotonation of [H**2′**]$^+$ by TEMPOH, the product of eq 5.[39] At 199 K, the rate of disappearance of [H**2′**]$^+$ proceeds at 8.13×10^{-3} $s^{-1}M^{-1}$. By measuring the temperature dependence of the rate constant over the range 199–229 K, we determined that $\Delta G^{\ddagger}$ is 13.5 kcal/mol (199 K). The secondary ammonium [H**2**]$^+$ was observed to react with TEMPO faster than did [H**2′**]$^+$ under similar conditions: the reaction was complete in minutes vs ~60 min for the Bn derivative at 199 K.

Insights into a possible mechanism of the hydrogen-atom transfer reactions were provided by experiments with the terminal hydrides $[HFe_2[(SCH_2)_2NR](CO)_2(dppv)_2]^+$ and $[HFe_2[(S_2C_3H_6)(CO)_2(dppv)_2]^+$.[6] In CH_2Cl_2 solution, both species were found to react ($t_{1/2}$ ≈ 10 min, −199 K) with TEMPO to give the corresponding mixed-valence Fe(II)Fe(I) derivatives.[25] The IR signatures for the diferrous hydride starting materials and mixed valence products overlap, thus we conducted these oxidations under an atmosphere of CO, which rapidly affords the CO adducts that display distinctive IR signatures.[25]

Conclusions

The hydrogenases function by coupling or combining acid-base and redox properties. The present study examined the interplay of these properties in a diiron model that contains both a base and a redox center. We report three unusual findings:

i. The mildness and reversibility of the $Fe^{II}Fe^{I}/Fe^{II}Fe^{II}$ couple in models containing the amine cofactor arises from the formation of an Fe-N bond.*[40, 41] Our measurements suggest that coordination of the amine stabilizes the diferrous state by ~11 kcal/mol as indicated by $\Delta E^{FeIIFeI/FeIIFeII}$.

*In the absence of the amine, 32e$^-$ diferrous dithiolates, e.g. analogues of $[Fe_2(S_2C_3H_6)(CO)_3(dppv)(PMe_3)]^{2+}$, are predicted to be stabilized by agostic interactions with the central methylene of the dithiolate. We expect that amine binding would be stronger than an agostic interaction, thus stabilizing this oxidation.

NIH-PA Author Manuscript

NIH-PA Author Manuscript

NIH-PA Author Manuscript

ii. The $Fe^{I}Fe^{I}$ ammonium center serves as an efficient H-atom donor, with concomitant Fe-centered redox. This finding demonstrates the ability of hydrogenase models and, by implication, the enzyme to participate in PCET.

iii. The basicity of the amine is highly sensitive to the oxidation state of the underlying diiron centers. The behavior of the mixed valence ammonium centers in models and in proteins may be quite different owing to the effects of site isolation provided by the protein.

The [FeFe]-hydrogenases are characterized by reduced and oxidized states, respectively H_{red} and H_{ox} that differ by $1e^{-}$. In terms of enzyme mechanism, the reduced state activates protons and the oxidized state activates H_2. The oxidation state for the diiron center in H_{red} remains uncertain, but is likely either a diferrous hydride or a disubferrous ammonium which would be readily interconverted.[6] As we demonstrated in this work, H_{red} and H_{ox} are separated formally as well as operationally by $H^{\cdot}$.

Our measurements bear on the mechanism for activation of H_2. In the heterolytic pathway which is assumed for all hydrogenases,[26] H_2 is a source of H^{-}, invariably bound to a Fe(II), and H^{+}, which is usually bound to an organic base. We show that the binding of hydride to Fe(II)Fe(I) complexes is far less favorable than to Fe(II)Fe(II) derivatives (Figure 6). The hydride acceptor strength of $[\mathbf{2}']^{+}$, −48 kcal/mol, is insufficient to compensate for the energy required for the heterolysis of H_2. Thus H_2 activation by $[\mathbf{2}']^{+}$ is predicted to be unfavorable, even when coupled to the neutralization of the proton by a moderately strong base.

The hydride acceptor strength of the diferrous center, e.g., $[\mathbf{2}']^{2+}$ (assuming κ^2-adt), −88 kcal/mol, *is* sufficiently exergonic that H_2 heterolysis is favorable. No biophysical evidence exists, however, for unsaturated diferrous state for the enzyme. In fact, Nature might avoid this state because it would be unstable with respect to coordination of the amine. The $2e^{-}$ change required for exergonic H_2 activation can however proceed via a PCET pathway,[42] avoiding formation of the Lewis acidic diferrous state. In this scenario, the appended 4Fe-4S cluster is poised to provide the oxidizing equivalent (eq 6). PCET has recently been proposed for other hydrogen redox reactions.[3]

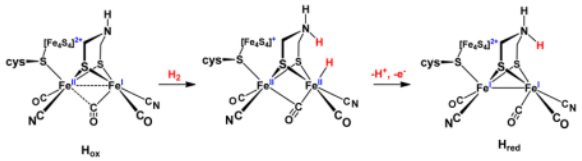

(6)

The relevance of PCET pathways is reinforced by the facile transfer of $H^{\cdot}$ from the ammonium and hydride tautomers of the diiron dithiolates, $[Fe_2[(SCH_2)_2NHR](CO)_3(dppv)(PMe_3)]^{+}$ and $[HFe_2(SR)_2(CO)_2(dppv)_2]^{+}$, respectively.

The κ^3-aminodithiolate ligand may be relevant to recent observations on the [FeFe]-hydrogenases. Upon being oxidized at ~0 V (vs SHE), the enzyme from *D. desulfuricans* reversibly deactivates to a state that is protected against oxidative (aerobic) damage.[43, 44] It is assumed that this protection is provided by a ligand that occupies the apical site on the distal Fe. Although this blocking ligand might be water or hydroxide,[2, 43] the amine could also serve this protective role. To the best of our knowledge, there are no reports that have addressed the feasibility of Fe-N bond formation within the enzyme or whether the cavity in which the H-cluster resides could accommodate an the elongation of the Fe-Fe distance.

NIH-PA Author Manuscript

NIH-PA Author Manuscript

NIH-PA Author Manuscript

Although we observe the Fe-Fe distance to increase by ~1 Å in [**2′**(MeCN)]$^{2+}$ relative to standard H_{ox} models,[12, 13] this may simply be to accommodate the size of the exogenous ligand, MeCN. Other unsaturated diferrous complexes show Fe-Fe distance elongation of only ~0.3 Å.[40]

Materials and Methods

Synthetic methods for $Fe_2[(SCH_2)_2(NBn)(CO)_3(dppv)(PMe_3)]$ have been recently described.[9] In situ IR measurements employed a React-IR 4000 (Mettler-Toledo). Compounds **2**[45], **2′**,[9] $FcBAr^F{}_4$,[46] and $H(OEt_2)_2BAr^F{}_4$[47] were prepared as previously reported. 2,2,6,6-Tetramethylpiperidine 1-oxyl (TEMPO) and $Cp^*{}_2Co$ were purchased from Sigma Aldrich and sublimed before use. Rate constants were obtained by simulation of experimental data using the program Kintecus.[48]

Protonation of $[Fe_2[(SCH_2)_2NBn](CO)_3(dppv)(PMe_3)]BAr^F{}_4$

To a solution of 0.025 g (0.029 mmol) of **2′** in 5 mL of CH_2Cl_2 was added a solution of 0.030 g (0.029 mmol) $FcBAr^F{}_{24}$ in 5 mL of CH_2Cl_2. The resulting purple solution was thermally equilibrated in an acetone/CO_2 bath for 10 min.. A solution of 0.014 g (0.015 mmol) $H(OEt_2)_2BAr^F{}_4$ in 2 mL of CH_2Cl_2 was added to the reaction mixture. The solution immediately became orange in color and the IR spectrum indicated the presence of only [**2′**] $(BAr^F{}_4)_2$ and [H**2′**]$BAr^F{}_4$ (see Figure 4). The presence of [H**2′**]$^+$ was confirmed by allowing it to isomerize to its μ-H counterpart. Upon warming to 20 °C, the reaction mixture was filtered through Celite, and the high-field ^{1}H NMR spectrum (CD_2Cl_2) confirmed the presence of [**2′**(μ-H)]$^+$. Under analogous conditions, a solution of [**1**]$BAr^F{}_4$ in CH_2Cl_2 was shown by IR spectroscopy to be unaffected by the addition of $H(OEt_2)_2BAr^F{}_4$, even after warming to 25 °C.

$[Fe_2[(SCH_2)_2NBn](CO)_3(dppv)(PMe_3)](BAr^F{}_4)_2$

Into a J.Young NMR tube containing 0.010 g (0.012 mmol) of **2′** and 0.025 g (0.023 mmol) of $FcBAr^F{}_4$, immersed in liquid N_2, was distilled 1 mL of CD_2Cl_2. The frozen mixture was thawed in a acetone/CO_2 bath and mixed, with care not to let the contents leave the cold bath. The tube was then quickly inserted into a spectrometer probe pre-cooled to −70 °C. Several hundred scans were necessary for a well-resolved spectrum. ^{31}P NMR (CD_2Cl_2, −70 °C): δ 77.0 (s, dppv), 44.1 (s, PMe_3).

$[Fe_2[(SCH_2)NBn](CO)_3(dppv)(PMe_3)(CD_3CN)](BAr^F{}_4)_2$

A solution of [**2′**]$(BAr^F{}_{24})_2$ in CD_2Cl_2 was generated in a J. Young NMR tube as described above. The solution was frozen, re-evacuated, and onto it was distilled 0.1 mL of CD_3CN. The tube was thawed in an acetone/CO_2 bath and re-inserted into the probe, which was pre-cooled to −70 °C. ^{31}P NMR (CD_2Cl_2, −70 °C): δ 73.5 (d, dppv, $J_{P\text{-}P}$ = 11 Hz, isomer A), 73.0 (s, dppv, isomer A), 20.8 (d, J = 11 Hz, PMe_3, isomer A). Chemical shifts vary slightly from the isolated complex due to change in counterion (BF_4^- vs $BAr^F{}_4^-$). ESI-MS: *m/z* 432.9 ($[Fe_2[(SCH_2)_2(NBn)(CO)_3(dppv)(PMe_3)]^{2+}$), 454.9, 619.4 ($[FeCl(CO)_2(dppv)(PMe_3)]^+$), ($[Fe_2[(SCH_2)_2NBn](CO)_3(dppv)(PMe_3)(CD_3CN)]^{2+}$), 900.7 ($[Fe_2[(SCH_2)_2NBn]Cl(CO)_3(dppv)(PMe_3)]^+$).

$Fe_2[(SCH_2)_2NBn](CO)_4(dppv)(PMe_3)](BAr^F{}_4)_2$ ([**2′CO**]$(BAr^F{}_4)_2$)

A solution of [**2′**]$(BAr^F{}_4)_2$ in CD_2Cl_2 was generated in a J. Young valve NMR tube as described above. The solution was frozen, re-evacuated, and pressurized with 1 atm of CO. The tube was thawed in an acetone/CO_2 bath and then slowly warmed to 20 °C. ^{31}P NMR (CD_2Cl_2, 20 °C): δ 68.4 (m, dppv), 68.2 (m, dppv), 15.7 (d, J = 11 Hz, PMe_3). ESI-MS: *m/z*

NIH-PA Author Manuscript

NIH-PA Author Manuscript

NIH-PA Author Manuscript

446.9 ($[Fe_2[(SCH_2)_2NBn](CO)_3(dppv)(PMe_3)(CO)]^{2+}$), 619.4 ($[FeCl(CO)_2(dppv)(PMe_3)]^+$), 900.7 ($[Fe_2[(SCH_2)_2NBn]Cl(CO)_3(dppv)(PMe_3)]^+$).

Treatment of [2′](BAr$^F_4$)$_2$ with $PhSiH_3$

A mixture of 0.050 g (0.058 mmol) [**2′**](BAr$^F_{24}$)$_2$ and 0.121 g (0.116 mmol) FcBAr$^F_{24}$ was cooled in an acetone/CO_2 bath, and to it was added 2 mL of CH_2Cl_2. In situ IR spectra indicated the presence of [**2′**](BAr$^F_{24}$)$_2$. IR (CH_2Cl_2): 2066, 2008, 1977. To this mixture was added 0.2 mL of $PhSiH_3$. After ~30 min, the [**2′**](BAr$^F_4$)$_2$ had been consumed. After warming to 20 °C, the sample was found to be spectroscopically (^{31}P, ^{1}H, IR, ESI-MS) identical to $[Fe_2(\mu\text{-}H)[(SCH_2)_2NBn](CO)_3(dppv)(PMe_3)(CO)]BAr^F_4$.[9]

Oxidation of $[Fe_2[(SCH_2)_2N(H)R](CO)_3(dppv)(PMe_3)]BAr^F_4$ with TEMPO (R = H, Bn)

A solution of [**2′**H]BAr$^F_4$ was generated at −78 °C by the addition of 0.8 mL of CH_2Cl_2 to a mixture of 0.023 g (0.027 mmol) of **2′** and 0.027 g (0.027 mmol) of $H(OEt_2)_2BAr^F_4$. Treatment of this solution with 0.103 g (0.66 mmol) of TEMPO gave [**2′**]$^+$. Similar spectra were obtained using [**2**H]$^+$ in place of [**2′**H]$^+$. We independently confirmed by IR spectroscopy that [**2′**H]$^+$ was fully deprotonated by 1 equiv of TEMPOH, the organic product of the H-atom transfer reaction (see eq 3). In a related experiment, we found that exposure of a solution of TEMPOH and [**2′**H]$^+$ to air rapidly gave [**2**]$^+$. Precautions were taken to avoid this facile aerobic oxidation pathway.

$[Fe_2[(SCH_2)_2NBn](CO)_3(dppv)(PMe_3)(MeCN)](BF_4)_2$

Obtaining single crystals of salts derived from [**2′**]$^{2+}$ proved challenging. Various counterions (BF_4^-, SbF_6^-, $BAr^F_4^-$, and BPh_4^-) and various solvent combinations (slow diffusion at −30 °C of hexanes, Et_2O, or toluene into CH_2Cl_2 solutions of the respective salts of [**2′**]$^{2+}$) all afforded amorphous tacky solids. We thus turned to the adduct, [**2′**(MeCN)]$^{2+}$. To a Schlenk tube containing a mixture of 0.050g (0.06 mmol) **2′** and 0.032 g (0.12 mmol) of $FcBF_4$, cooled to −78 °C, was added 8 mL of CH_2Cl_2. The solution was stirred vigorously for 5 min, and then 0.1 mL of MeCN was added. Stirring was stopped, and 40 mL of hexane was carefully layered on top of the reaction mixture and allowed to diffuse at −30 °C. After ~4 days, red crystals had formed. The supernatant was filtered off to remove ferrocene and then the crystalline solid was scrapped from the flask. Finally, this material was dried *en vacuo*, extracted into 5 mL of CH_2Cl_2, filtered through Celite, and precipitated as an orange-colored powder upon the addition of 20 mL of hexanes. IR (CH_2Cl_2, cm^{-1}): ν_{CO} = 2065, 2042, 2001, 1974. ^{31}P NMR (CD_2Cl_2, 20 °C): δ 73.0 (s, dppv, isomer A), 72.9 (d, dppv, $J_{P\text{-}P}$ = 13 Hz, isomer A), 21.3 (d, J = 13 Hz, PMe_3, isomer A. ^{31}P NMR (CD_2Cl_2, 48 h at 20 °C): δ 79.9 (s, dppv, isomer B), 25.8 (s, PMe_3, isomer B). MS ESI: *m/z* = 453.2 ($[Fe_2[(SCH_2)_2NBn](CO)_3(dppv)(PMe_3)(MeCN)]^{2+}$). The dppv P-Fe-P coupling is not resolved (J<5 Hz), instead the dppv signal is broadened (FWHH = 14 Hz). Anal. Calcd (Found) for $C_{43}H_{45}B_2F_8Fe_2N_2O_3P_3S_2$: C, 47.81 (47.09); H, 4.20 (4.41); N, 2.59 (2.40).

Single crystals were obtained from 8 mL of CH_2Cl_2 solution of 7 mM [**2′**](BF$_4$)$_2$, which was generated at −78 °C as described above and then treated with 5 drops of MeCN. The solution was then layered with 50 mL of hexane and stored at −30 °C. After 1 week, several red crystals had appeared. Alternatively, a 7 mM solution of [**2′**]BF$_4$ was treated with 1 drop of MeCN and then layered with 50 mL of hexane. After 1 week, a single cluster of red crystals had formed and were separated from the dark brown solution.

NIH-PA Author Manuscript

NIH-PA Author Manuscript

NIH-PA Author Manuscript

Crystallography

Structure was phased by dual space methods. Systematic conditions suggested the ambiguous space group P1-. The space group choice was confirmed by successful convergence of the full-matrix least-squares refinement on F^2. The highest peak in the final difference Fourier map was located 2.6 Å from the nearest aromatic H atom. This residual density located in a void suggests the possibility of a partially occupied water solvate. The final map had no other significant features. A final analysis of variance between observed and calculated structure factors showed no dependence on amplitude or resolution. The proposed model includes two disordered positions for phenyl ring C20–25 of the host cation and two disordered positions for one of two CH_2Cl_2 solvate molecules. Phenyl rings were refined as rigid, idealized groups. A common geometry was imposed on the disordered CH_2Cl_2 solvates using effective standard deviations of 0.01 and 0.02 Å for bond lengths and bond angles, respectively. Rigid-bond restraints (esd 0.01) were imposed on displacement parameters for all disordered sites and similar displacement amplitudes (esd 0.01) were imposed on disordered sites overlapping by less than the sum of van der Waals radii. Methyl H atom positions were optimized by rotation about R-C bonds with idealized C-H, R-H and H---H distances. Remaining H atoms were included as riding idealized contributors. Methyl H atom *U*'s were assigned as 1.5 times U_{eq} of the carrier atom; remaining H atom *U*'s were assigned as 1.2 times carrier U_{eq}.

Electrochemistry

Cyclic voltammetry experiments were carried out in a ~10 mL scintillation vial inside of an anaerobic dry glove box. The working electrode was a glassy carbon disk (0.3 cm in diameter), the pseudo-reference electrode an Ag wire, and the counter electrode a Pt wire. Under our experimental conditions (CH_2Cl_2 solution), we generally observed that ΔE_p was ~0.12 V for the $[Fe_2]^{0/+}$ couple, whereas an equimolar internal standard of Fc displayed ΔE_p as ~0.1 V. All potentials were referenced versus the 0.001 M internal Fc standard.

Supplementary Material

Refer to Web version on PubMed Central for supplementary material.

Acknowledgments

This research was sponsored by NIH. MTO thanks the NIH for a CBI-Fellowship.

References

1. Kubas, GJ. Metal Dihydrogen and σ-Bond Complexes. Kluwer Academic/Plenum; New York: 2001. p. 472
2. Vincent KA, Parkin A, Armstrong FA. Chem Rev. 2007; 107:4366–4413. [PubMed: 17845060]
3. Rakowski DuBois M, DuBois DL. Chem Soc Rev. 2009; 38:62–72. [PubMed: 19088965]
4. Lubitz W, Reijerse E, van Gastel M. Chem Rev. 2007; 107:4331–4365. [PubMed: 17845059]
5. Silakov A, Wenk B, Reijerse EJ, Lubitz W. Phys Chem Chem Phys. 2009; 11:6592–6599. [PubMed: 19639134]
6. Barton BE, Olsen MT, Rauchfuss TB. J Am Chem Soc. 2008; 130:16834–16835. [PubMed: 19053433]
7. Peters JW, Lanzilotta WN, Lemon BJ, Seefeldt LC. Science. 1998; 282:1853–1858. [PubMed: 9836629]
8. Nicolet Y, de Lacey AL, Vernede X, Fernandez VM, Hatchikian EC, Fontecilla-Camps JC. J Am Chem Soc. 2001; 123:1596–1601. [PubMed: 11456758]
9. Olsen MT, Barton BE, Rauchfuss TB. Inorg Chem. 2009; 48:7507–7509. [PubMed: 19603776]

NIH-PA Author Manuscript

NIH-PA Author Manuscript

NIH-PA Author Manuscript

10. Tard C, Liu X, Ibrahim SK, Bruschi M, De Gioia L, Davies SC, Yang X, Wang LS, Sawers G, Pickett C. J Nature. 2005; 433:610–614.
11. Tye JW, Darensbourg MY, Hall MB. Inorg Chem. 2006; 45:1552–1559. [PubMed: 16471966]
12. Justice AK, Rauchfuss TB, Wilson SR. Angew Chem Int Ed. 2007; 46:6152–6154.
13. Justice AK, De Gioia L, Nilges MJ, Rauchfuss TB, Wilson SR, Zampella G. Inorg Chem. 2008; 47:7405–7414. [PubMed: 18620387]
14. Liu T, Darensbourg MY. J Am Chem Soc. 2007; 129:7008–7009. [PubMed: 17497786]
15. Thomas CM, Liu T, Hall MB, Darensbourg MY. Inorg Chem. 2008; 47:7009–7024. [PubMed: 18597449]
16. Olsen MT, Bruschi M, De Gioia L, Rauchfuss TB, Wilson SR. J Am Chem Soc. 2008; 130:12021–12030. [PubMed: 18700771]
17. Cheah MH, Tard C, Borg SJ, Liu X, Ibrahim SK, Pickett CJ, Best SP. J Am Chem Soc. 2007; 129:11085–11092. [PubMed: 17705475]
18. Eilers G, Schwartz L, Stein M, Zampella G, De Gioia L, Ott S, Lomoth R. Chem Eur J. 2007; 13:7075–7084.
19. Ezzaher S, Orain P, Capon J, Gloaguen F, Petillon F, Roisnel T, Schollhammer P, Talarmin J. Chem Comm. 2008:2547–2549. [PubMed: 18506239]
20. Barton BE, Zampella G, Justice AK, De Gioia L, Rauchfuss TB, Wilson SR. Dalt Trans. 2009 Advance Article.
21. Fontecilla-Camps JC, Volbeda A, Cavazza C, Nicolet Y. Chem Rev. 2007; 107:4273–4303. [PubMed: 17850165]
22. Siegbahn PEM, Tye JW, Hall MB. Chem Rev. 2007; 107:4414–4435. [PubMed: 17927160]
23. Zhao X, Chiang CY, Miller ML, Rampersad MV, Darensbourg MY. J Am Chem Soc. 2003; 125:518–524. [PubMed: 12517165]
24. van der Vlugt JI, Rauchfuss TB, Wilson SR. Chem Eur J. 2005; 12:90–98.
25. Justice AK, Nilges MJ, Rauchfuss TB, Wilson SR, De Gioia L, Zampella G. J Am Chem Soc. 2008; 130:5293–5301. [PubMed: 18341276]
26. Kubas GJ. Chem Rev. 2007; 107:4152–4205. [PubMed: 17927158]
27. Landau SE, Morris RH, Lough AJ. Inorg Chem. 1999; 38:6060–6068. [PubMed: 11671314]
28. Henry RM, Shoemaker RK, Dubois DL, Rakowski Dubois M. J Am Chem Soc. 2006; 128:3002–3010. [PubMed: 16506781]
29. Lawrence JD, Li H, Rauchfuss TB, Bénard M, Rohmer MM. Angew Chem, Int Ed. 2001; 40:1768–1771.
30. Ott S, Kritikos M, Åkermark B, Sun L, Lomoth R. Angew Chem, Int Ed. 2004; 43:1006–1009.
31. Dong W, Wang M, Liu X, Jin K, Li G, Wang F, Sun L. Chem Commun. 2006:305–7.
32. Boyke CA, Rauchfuss TB, Wilson SR, Rohmer MM, Bénard M. J Am Chem Soc. 2004; 126:15151–15160. [PubMed: 15548012]
33. Boyke CA, van der Vlugt JI, Rauchfuss TB, Wilson SR, Zampella G, De Gioia L. J Am Chem Soc. 2005; 127:11010–11018. [PubMed: 16076208]
34. van der Vlugt JI, Rauchfuss TB, Whaley CM, Wilson SR. J Am Chem Soc. 2005; 127:16012–16013. [PubMed: 16287273]
35. Geiger WE, Barriere F. Acc Chem Res. 2010; 43:1030–1039. [PubMed: 20345126]
36. Heiden ZM, Rauchfuss TB. J Am Chem Soc. 2009; 131:3593–3600. [PubMed: 19236021]
37. Li T, Lough AJ, Morris RH. Chem Eur J. 2007; 13:3796–3803.
38. Anelli PL, Biffi C, Montanari F, Quici S. J Org Chem. 1987; 52:2559–2562.
39. Sen VD, Golubev VA. J Phys Org Chem. 2008; 22:138–143.
40. Bruschi M, Fantucci P, De Gioia L. Inorg Chem. 2003; 42:4773–4781. [PubMed: 12870970]
41. Geiger WE, Ohrenberg NC, Yeomans B, Connelly NG, Emslie DJH. J Am Chem Soc. 2005; 125:8680–8688. [PubMed: 12848576]
42. Mayer JM. Annual Review of Physical Chemistry. 2004; 55:363–390.

NIH-PA Author Manuscript

NIH-PA Author Manuscript

NIH-PA Author Manuscript

43. Vincent KA, Parkin A, Lenz O, Albracht SPJ, Fontecilla-Camps JC, Cammack R, Friedrich B, Armstrong FA. J Am Chem Soc. 2005; 127:18179–18189. [PubMed: 16366571]
44. van Dijk C, van Berkel-Arts A, Veeger C. FEBS Lett. 1983; 156:340–344.
45. Justice AK, Zampella G, De Gioia L, Rauchfuss TB, van der Vlugt JI, Wilson SR. Inorg Chem. 2007; 46:1655–1664. [PubMed: 17279743]
46. Le Bras J, Jiao H, Meyer WE, Hampel F, Gladysz JA. J Organomet Chem. 2000; 616:54–66.
47. Brookhart M, Grant B, Volpe AF Jr. Organometallics. 1992; 11:3920–3922.
48. Ianni J. Kintecus. 3.962

NIH-PA Author Manuscript

NIH-PA Author Manuscript

NIH-PA Author Manuscript

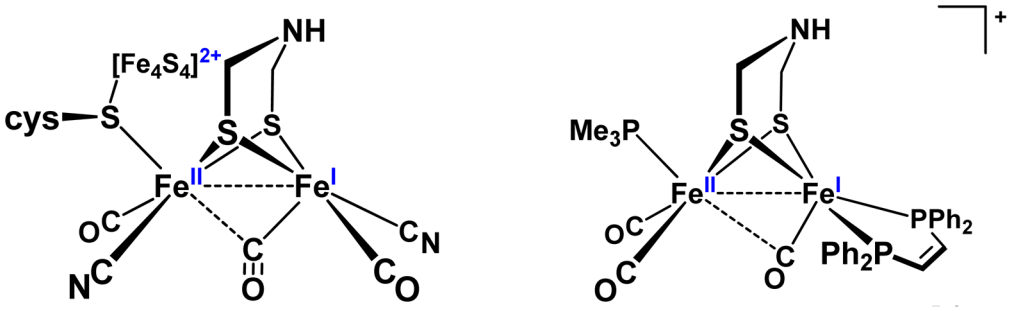

Figure 1.

Active site of the oxidized state (H_{ox}) of the [FeFe]-hydrogenase (left),[7, 8] showing the azadithiolate cofactor and a vacant site on the distal iron center.[9] Model complex for the H_{ox} state of the active site, with organophosphorus ligands in place of the cyanide and 4Fe-4S cofactors.

NIH-PA Author Manuscript

NIH-PA Author Manuscript

NIH-PA Author Manuscript

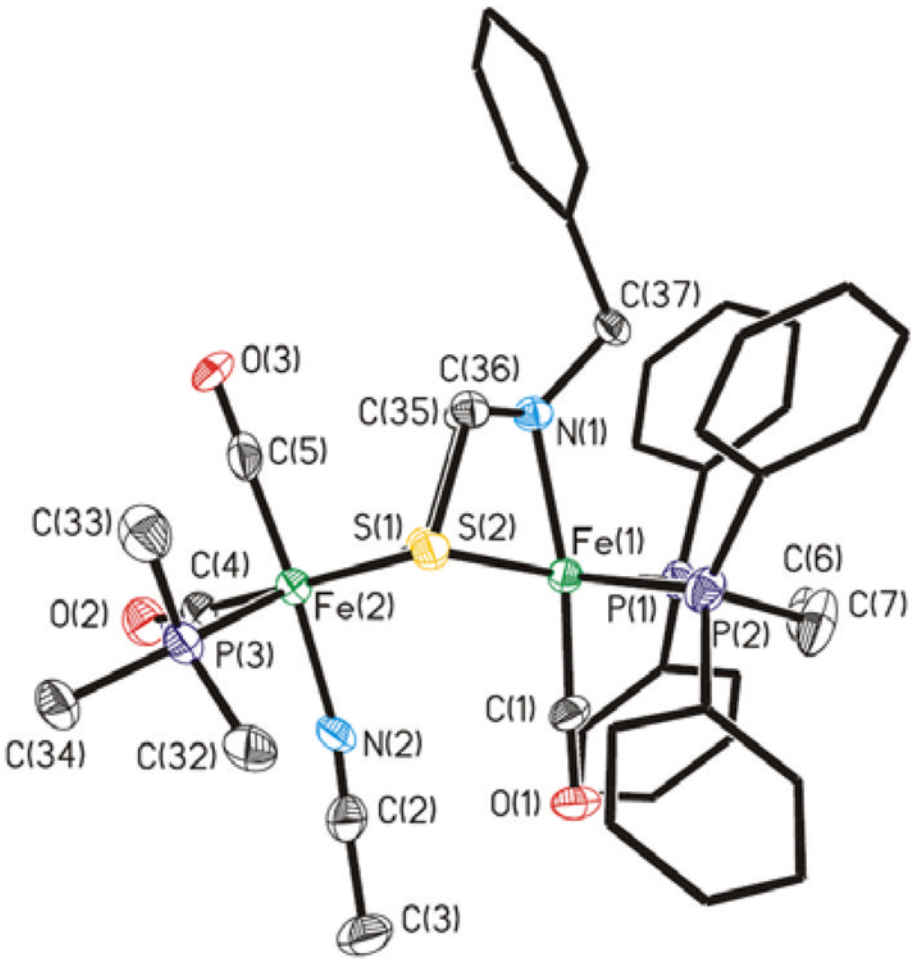

Figure 2.
Structure of the dication in [**2′**(NCMe)]$(BF_4)_2$. Thermal ellipsoids set at the 30% probability level and hydrogen atoms are not shown.

NIH-PA Author Manuscript

NIH-PA Author Manuscript

NIH-PA Author Manuscript

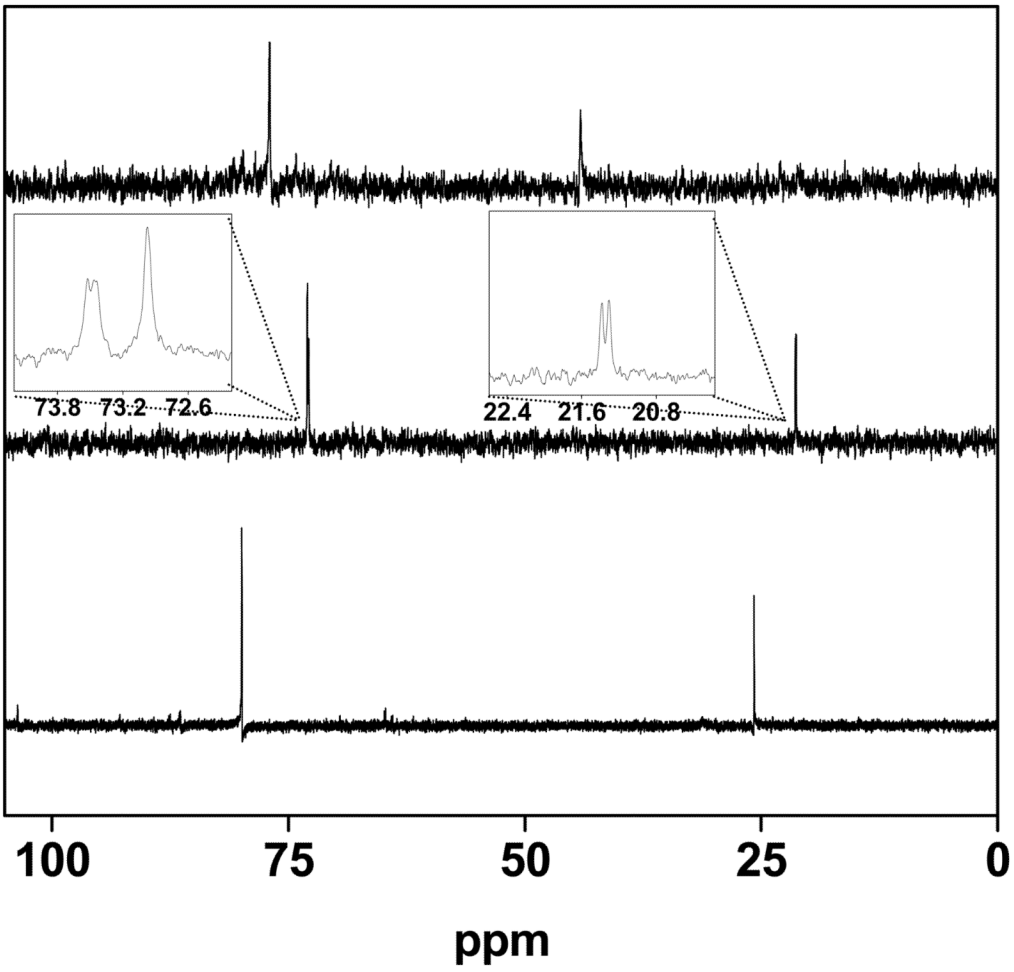

Figure 3.

^{31}P NMR spectra (CD_2Cl_2) of a fresh solution of [**2′**]($BAr^F{}_4$)$_2$ at −193 K (top), after treatment with CD_3CN (middle), and after allowing the same solution to stand at 293 K for 48 h. Signals at > δ70 are assigned to dppv and those absorbing < δ40 are assigned to PMe_3. The former signals are more indicative of symmetry and the latter signals are useful indicators of the number of isomers.

NIH-PA Author Manuscript

NIH-PA Author Manuscript

NIH-PA Author Manuscript

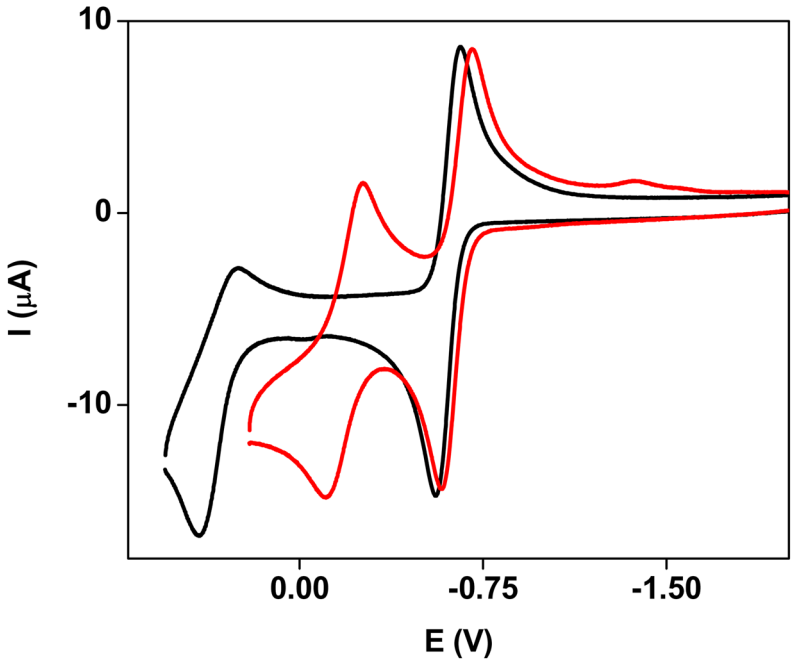

Figure 4.

Cyclic voltammograms of a CH_2Cl_2 solution of **1** (black) and **2′** (red) illustrative of the effect of the azadithiolate on the second anodic event. *Conditions:* 0.001 M **2′**, 0.300 M $[(C_4H_9)_4N]PF_6$, CH_2Cl_2, 20 °C, 0.1 V/s scan rate.

NIH-PA Author Manuscript

NIH-PA Author Manuscript

NIH-PA Author Manuscript

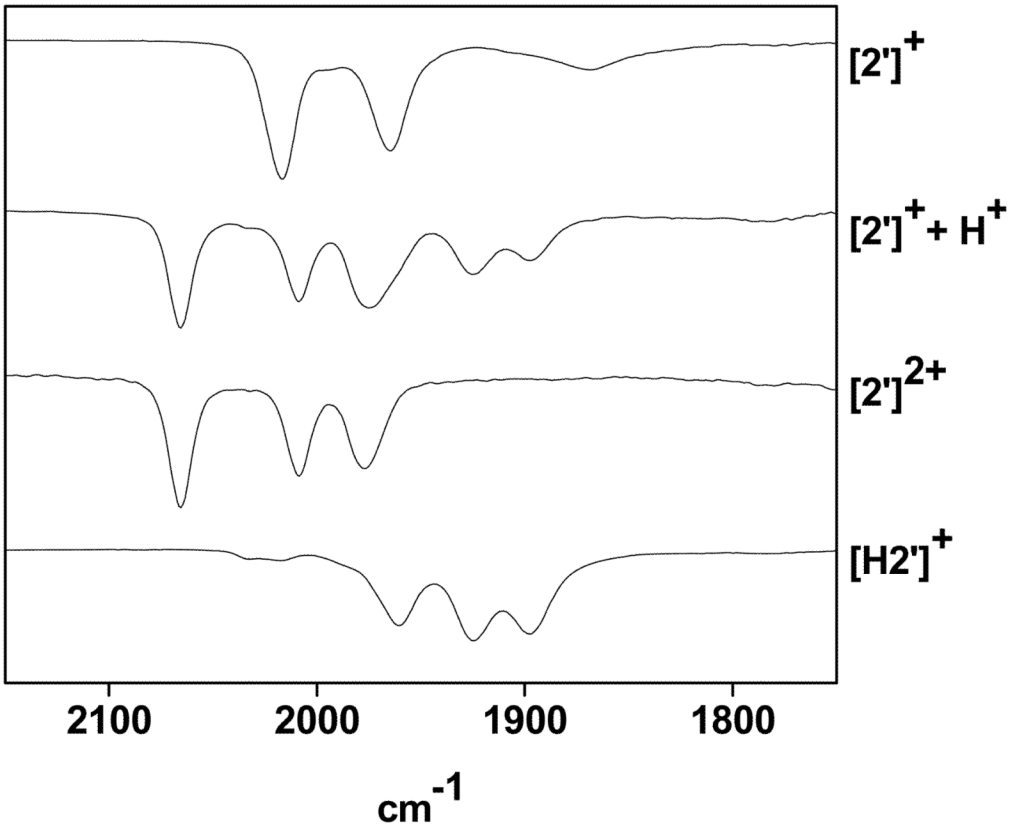

Figure 5.

IR spectra (CH_2Cl_2 solution) for [**2′**]$^+$ (top), the products of its reaction with 0.5 equiv of $H(OEt_2)_2BAr^F{}_4$ (middle top), [**2′**]$(BAr^F{}_{24})_2$ (middle bottom), [H**2′**]$^+$ generated by protonation of **2′** with $H(OEt_2)_2BAr^F{}_{24}$ (bottom). Component IR bands (CH_2Cl_2) are [**2′**]$^+$: 2017, 1965, 1867 cm^{-1}; [**2′**]$^{2+}$: 2065, 2009, 1977; [H**2′**]$^+$: 1960, 1925, 1898 cm^{-1}.

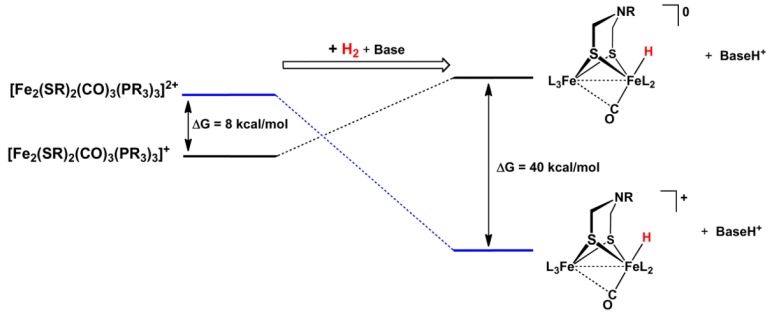

Figure 6.

Free energy changes (vs $E(Fc^{0/+}) = 0$ V) for the hydrogenation of mixed-valence and diferrous dithiolato complexes using data obtained for $[Fe_2[(SCH_2)_2NR](CO)_3(dppv)(PMe_3)]^n$ (n = +, 2+). The calculation assumes that the proton binds to a base of pK_a^{MeCN} = 10.

NIH-PA Author Manuscript NIH-PA Author Manuscript NIH-PA Author Manuscript

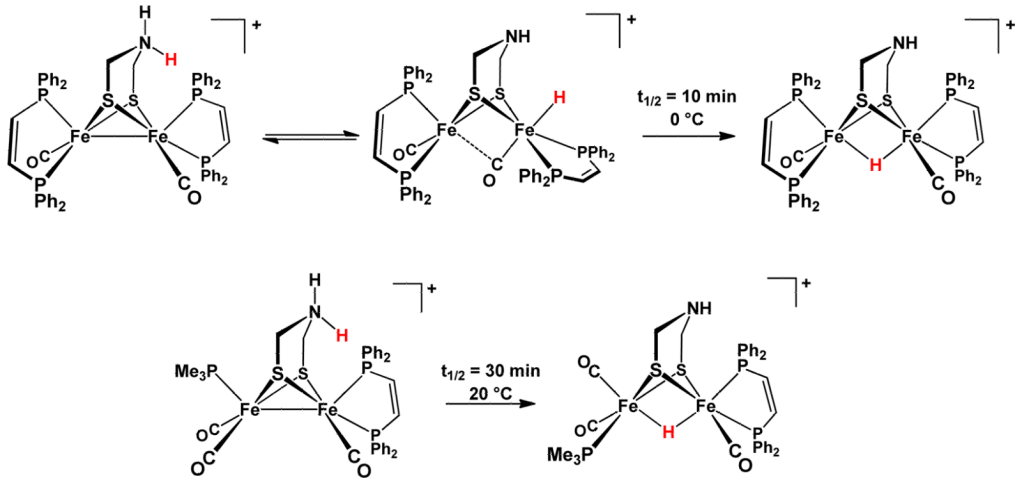

Scheme 1.
Regiochemistry of protonation of tri- and tetrasubstituted diiron azadithiolato carbonyl complexes.[6, 9]

NIH-PA Author Manuscript
NIH-PA Author Manuscript
NIH-PA Author Manuscript

NIH-PA Author Manuscript

NIH-PA Author Manuscript

NIH-PA Author Manuscript

$$[\mathbf{2'}]^{+} + e^{-} \rightarrow \mathbf{2'} \qquad \Delta G = 23.06(E_{1/2}) = 13.8 \text{ kcal/mol}$$

$$[\mathbf{2'}]^{+} + H^{+} \rightarrow [H\mathbf{2'}]^{2+} \qquad \Delta G = 8.4 \text{ kcal/mol} = -1.37(pK_a^{CD_2Cl_2})$$

$$pK_a^{CD_2Cl_2} = -6.1$$

Scheme 2.

Bordwell calculation at 20 °C of the $pK_a^{CD_2Cl_2}$ of $[H\mathbf{2'}]^{2+}$ assuming $E_{1/2}$ of the $[H\mathbf{2'}]^{+/2+}$ couple as 0.04 V.

NIH-PA Author Manuscript

NIH-PA Author Manuscript

NIH-PA Author Manuscript

Table 1

Selected Bond Distances (Å) and Angles (°) for [2′(MeCN)]$(BF_4)_2$

bond	distance	bonds	angles
Fe(1)-N(1)	2.098(8)	N(1)-Fe(1)-S(2)	72.9(2)
Fe(1)-Fe(2)	3.477(2)	Fe(1)-S(2)-C(36)	80.9(3)
Fe(1)-C(1)	1.753(11)	Fe(2)-S(2)-C(36)	107.7(4)
Fe(2)-N(2)	1.965(10)	S(1)-Fe(1)-S(2)	80.97(11)
Fe(1)-S(2)	2.336(3)	S(1)-Fe(2)-S(2)	81.45(11)
Fe(2)-S(2)	2.323(3)	P(1)-Fe(1)-P(2)	87.24(12)

NIH-PA Author Manuscript

NIH-PA Author Manuscript

NIH-PA Author Manuscript

Table 2

Half-wave Potentials (V) for the $[Fe_2(SR)_2]^{0/+}$ and $[Fe_2(SR)_2]^{+/2+}$ Couples for $Fe_2[(SCH_2)_2X](CO)_3(dppv)(PMe_3)$. *Conditions:* 1 mM diiron complex, 100 mM $[Bu_4N]PF_6$, CH_2Cl_2 Solution, vs $Fc^{0/+}$, 0.1 V/s scan rate. Under our experimental conditions, an internal standard of Fc (1 mM) displayed $\Delta E_p \approx 100$ mV. The i_{pa}/i_{pa} values for E_1 were recorded under conditions where the scan range did not extend to E_2

Dithiolate	Electrolyte	E_1 for $[Fe_2(SR)_2]^{0/+}$ (ΔE_p, V) [i_{pc}/i_{pa}]	E_2 for $[Fe_2(SR)_2]^{+/2+}$ (ΔE_p) [i_{pc}/i_{pa}]	$E_2 - E_1$
$(SCH_2)_2NBn$ (**2′**)	$[(C_4H_9)_4N]PF_6$	−0.643 0.118) [>0.9]	−0.128 (0.147) [>0.9]	0.515
$(SCH_2)_2NBn$ (**2′**)	$[(C_4H_9)_4N]BAr^F{}_4$	−0.715 (0.111) [0.9]	−0.070 (0.222) [0.7][b]	0.645
$(SCH_2)_2NH$ (**2**)	$[(C_4H_9)_4N]PF_6$	−0.561 (0.095) not determined[a]	−0.363 (0.101) not determined[a]	0.198
$(SCH_2)_2NH$ (**2**)	$[(C_4H_9)_4N]BAr^F{}_4$	−0.624 (0.075) [>0.9]	−0.249 (0.175) [0.1][b]	0.375
$(SCH_2)_2CH_2$ (**1**)	$[(C_4H_9)_4N]PF_6$	−0.609 (0.126) [>0.9]	0.356 (0.160) [0.2]	0.965
$(S_2C_2H_4)$	$[(C_4H_9)_4N]PF_6$	−0.469 (0.121) [>0.9]	0.345 (0.143) [0.5]	0.930
$(SCH_2)_2O$ (**3**)	$[(C_4H_9)_4N]PF_6$	−0.528 (0.139) [>0.9]	0.353 (0.233) [0.1]	0.840
$[(SCH_2)_2NBn(H)]^+$ ($[H\mathbf{2}']^+$)	$[(C_4H_9)_4N]PF_6$	$E_{p/2}$ = 0.040 (irrev.)	---	---
$[(SCH_2)_2NH_2]^+$ ($[H\mathbf{2}]^+$)	$[(C_4H_9)_4N]PF_6$	$E_{p/2}$ = 0.050 (irrev.)	---	---

[a] The close separation of the two oxidation steps precludes accurate measurement of this current ratio.

[b] At fast scan rates the cathodic return wave of $\mathbf{E}_2$ becomes broadened making the i_{pc}/i_{pa} value an inaccurate representation of reversibility. At slow scan rates $\mathbf{E}_2$ is fully reversible.

NIH-PA Author Manuscript

NIH-PA Author Manuscript

NIH-PA Author Manuscript

Table II

Estimated Affinities of $[2']^+$ for H^+, $H^{\cdot}$, and H^- (kcal/mol) in MeCN Solution (20 °C)

$\Delta G(H^+)$	$\Delta G(H^{\cdot})$	$\Delta G(H^-)$
15	−56	−48